International Journal of Solids and Structures 45 (2008) 4879–4901

Contents lists available at ScienceDirect

International Journal of Solids and Structures

journal homepage: www.elsevier.com/locate/ijsolstr

Elastic stress distributions for hyperbolic and parabolic notches in round shafts under torsion and uniform antiplane shear loadings

M. Zappalorto [a], P. Lazzarin [a], J.R. Yates [b,*]

[a] Dipartimento di Tecnica e Gestione dei Sistemi Industriali, Università di Padova, stradella San Nicola, 3-36100 Vicenza, Italy
[b] Department of Mechanical Engineering, University of Sheffield, Mappin Street, Sheffield S1 3JD, United Kingdom

ARTICLE INFO

Article history:
Received 29 October 2007
Received in revised form 22 February 2008
Available online 3 May 2008

Keywords:
Notch
Stress distribution
Antiplane shear loading
Torsion
Notch stress intensity factor
Strain energy density

ABSTRACT

Closed-form solutions are developed for the stress fields induced by circumferential hyperbolic and parabolic notches in axisymmetric shafts under torsion and uniform antiplane shear loading. The boundary value problem is formulated by using complex potential functions and two different coordinate systems, providing two classes of solutions. It is also demonstrated that some solutions of linear elastic fracture and notch mechanics reported in the literature can be derived as special cases of the general solutions proposed herein. Finally the analytical frame is used to link the Mode III notch stress intensity factor to the maximum shear stress at the notch tip, as well as to give closed-form expressions for the strain energy averaged over a finite size volume surrounding the notch root.

1. Introduction

Knowledge of the linear elastic stress fields ahead of notches is essential in the high cycle fatigue assessment of structural components. The most famous analytical contribution to the study of circumferentially blunt notched shafts under torsion is that due to Neuber (1958), who addressed the problem of '*deep*' and '*shallow*' notches and was able to determine in both cases the theoretical stress concentration factor K_t. Thanks to Neuber's solution, a number of plots for K_t related to common geometries under torsion were drawn (Peterson, 1974). Before Neuber, other authors had focused their attention to antiplane stress problems dealing with keyway grooved or longitudinally cracked cylindrical shafts (Filon, 1900; Shepherd, 1932; Wigglesworth and Stevenson, 1939; Wigglesworth, 1939). Some analytical tools reported in these papers will be reconsidered herein. In order to overcome some limitations of the analytical approaches, various numerical techniques have been used to obtain approximate solutions for the stress concentration factor of notched components subjected to torsion, see, amongst others, Rushton (1967), Hamada and Kitagawa (1968), Matthews and Hoke (1971) and Peterson (1974). Worthy of mention are also some recent contributions due to Noda and Takase who accurately determined, by means of the body force method, the stress concentration factors of blunt V-notches in round bars under torsion loading (Noda and Takase, 2006), as well as the notch stress intensity factors of sharp, zero radius, V-notches (Noda and Takase, 2003).

Considering the local stress distributions and not only K_t is essential in dealing with the structural integrity of notched components. Creager and Paris (1967) gave the elastic stress fields in the vicinity of the tip of blunt cracks, or '*slim*' parabolic notches, under Modes I, II and III loading. The intensities of the fields were expressed in terms of generalised stress intensity factors, later correlated by Glinka to the maximum elastic stress in plane problems (Glinka, 1985). A major difference of a

* Corresponding author.
E-mail address: j.yates@shef.ac.uk (J.R. Yates).

0020-7683/$ - see front matter © 2008 Published by Elsevier Ltd.
doi:10.1016/j.ijsolstr.2008.04.020

notch under Modes I and II loading compared with a cracked body, is that the bluntness of the notch results in the presence of stress terms proportional to $x^{0.5}$ and $x^{1.5}$, x being the distance from the notch tip. Under Mode III loading, only the term proportional to $x^{0.5}$ is present, and the analogy with the crack case is stronger.

The stress distribution problem for sharp V-shaped notches in round bars under antiplane shear was solved by Seweryn and Molski (1996), Dunn et al. (1997), and Qian and Hasebe (1997), who also dealt with the problem of the singularity at the interface of a bi-material V-notch.

Recently, the elastic stress fields ahead of semi-elliptic circumferential notches in infinite and finite size round bars under torsion were reported by the present authors (Lazzarin et al., 2007). The boundary value problem was formulated by using a complex potential function approach in combination with Inglis' elliptic coordinate system (Inglis, 1913). The solutions were found to have a wide range of applicability, both in terms of notch depth and notch shape. In particular, when the minor semi-axis b tends to zero, that is the crack case, Westergaard's stress function for mode III was obtained. Furthermore, it was possible to analyse with the same analytical framework the case of a semi-circular notch with a minor semi-axis b to major semi-axis a ratio equal to 1.0. The solution, exact in the case of a notch in an infinite diameter shaft, has been extended to a finite size shaft, making it possible to evaluate K_t as a function of a/b and a/R ratios, R being the shaft radius on the net transverse section. Finally, the case of a circumferential semi-elliptic notch at an arbitrary orientation angle β to the longitudinal axis of symmetry has been treated.

Confirming some findings by Smith (2004a,b,c), Lazzarin et al. (2007) also demonstrated that the distance over which stress distributions are dependent only on the root radius ρ, and not on the notch shape, is really very limited, and is approximately 0.05ρ. This is quite different to the case of notched components under Mode I loading where that distance of root radius dominance is much greater, about $0.2–0.3\rho$ (Nui et al., 1994; Atzori et al., 2001).

The main aim of the present work is to provide a set of closed-form solutions for stress, strain and displacement fields induced by hyperbolic and parabolic circumferential notches in axisymmetric shafts under torsion or uniform antiplane loading. The boundary value problems will be formulated according to the complex potential function approach, as in (Lazzarin et al., 2007), but using here hyperbolic and parabolic coordinate systems. It will be possible to provide two different classes of solutions whose accuracy and range of applicability will be discussed in detail taking advantage of a large number of results from FE analyses. The finite size effect on the elastic stress distributions will be considered as well. It will be also shown that some well-known solutions of linear elastic fracture mechanics and notch mechanics can be seen as special cases of the general solutions reported herein.

Finally, the developed analytical frame is used to tie the Mode III notch stress intensity factor (NSIF) to the maximum shear stress at the notch root, as well as to give closed-form expressions for the strain energy averaged over a given control volume embracing the notch root, the volume being exactly that defined in some recent contributions (Lazzarin and Berto, 2005; Gómez et al., 2007) where only plane cases have been considered (Mode I and mixed, I + II, loading). Those papers demonstrated that the averaged strain energy density made it possible to rationalise a large body of experimental data, despite the large variability of the notch root radius and opening angle.

2. Mathematical preliminaries

2.1. Fundamental complex potentials in antiplane elasticity

Consider an axisymmetric body weakened by a circumferential notch of a generic shape, made of an isotropic and homogenous material obeying the theory of linear elastic deformations. Consider also a Cartesian reference system (x,y,z) having the origin at an appropriate distance from the notch tip.

Suppose now that the body is loaded by a remote shear stress τ, resulting only in displacements w in the z direction, normal to the plane of the notch characterised by the x and y axes, as shown in Fig. 1.

Under these conditions the following relationships for stresses and strains are valid (Lazzarin et al., 2007):

$$\tau_{zx} - \mathrm{i}\tau_{zy} = H'(z), \tag{1}$$

$$\gamma_{zx} - \mathrm{i}\gamma_{zy} = \frac{H'(z)}{G}, \tag{2}$$

in Cartesian coordinates and

$$\tau_{zr} - \mathrm{i}\tau_{z\varphi} = \mathrm{e}^{\mathrm{i}\varphi}H'(z), \tag{3}$$

$$\gamma_{zr} - \mathrm{i}\gamma_{z\varphi} = \frac{\mathrm{e}^{\mathrm{i}\varphi}H'(z)}{G}, \tag{4}$$

in polar coordinates. Moreover the displacement w in the z direction can be determined as (Lazzarin et al., 2007):

$$w = \frac{\mathrm{Re}\{H(z)\}}{G}. \tag{5}$$

The function $H(z)$ is a holomorphic function of arbitrary form, which will vary from case to case depending on the relevant boundary conditions.

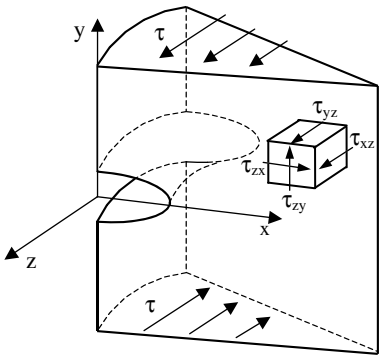

Fig. 1. Axis-symmetric body weakened by a circumferential notch and subjected to antiplane shear stresses.

Since stresses and displacements cannot change with a change of origin, in the absence of body forces, expressions (1)–(5) are independent of the choice of it. See, for example, Stevenson (1945) for plane problems.

So in the following study, we shall translate the origin of the reference system in the x-direction as a function of the notch shape and the transformation used, without any loss of generality.

Finally, it is worth noting that, according to the past literature, the symbol "z" is used in this paper with two different meanings that must not be confused; indeed it denotes both the complex variable $z = x + iy$ and the antiplane coordinate in the Cartesian reference system (x,y,z).

2.2. Hyperbolic coordinate system

We shall use here an orthogonal hyperbolic coordinate system generated by the transformation (Filon, 1900; Timoshenko and Goodier, 1970):

$$z = c\cosh\zeta, \tag{6}$$

where c is a constant and $z = x + iy$ and $\zeta = \xi + i\eta$ are complex variables in the physical and the transformed planes, respectively. In terms of the components x and y, Eq. (6) becomes:

$$x = c\cosh\xi\cos\eta, \quad y = c\sinh\xi\sin\eta \tag{7}$$

and so

$$\cosh\xi = \frac{x}{c\cos\eta}, \quad \sinh\xi = \frac{y}{c\sin\eta}. \tag{8}$$

Elimination of ξ requires:

$$\frac{x^2}{c^2\cos^2\eta} - \frac{y^2}{c^2\sin^2\eta} = 1. \tag{9}$$

Different values of η result in a family of hyperbolae, all characterised by the same foci, see Fig. 2a:

$$x = \pm\sqrt{c^2\cdot(\cos^2\eta + \sin^2\eta)} = \pm c. \tag{10}$$

When varying ξ, for $\eta = \eta_0$ and $\eta = -\eta_0$ in the first and fourth quadrants of the Cartesian plane, respectively, Eq. (9) describes a particular hyperbola of the family, see Fig. 2b.

Consider a hyperbolic profile characterised by the asymptotes $y = \pm\frac{b}{a}x$, intersecting the x-axis at the value $x = a$. The comparison between Eq. (9), setting $\eta = \eta_0$, and the canonical equation of an hyperbola results in:

$$\begin{cases} a = c\cos\eta_0 \\ b = c\sin\eta_0 \end{cases}. \tag{11}$$

Furthermore the following relations are also valid:

$$\begin{cases} b = \sqrt{c^2 - a^2} \\ \eta_0 = \arctan\left(\frac{b}{a}\right) \end{cases}. \tag{12}$$

Inverting Eq. (6), being x and y both positive, results in (Lazzarin et al., 2007):

$$\zeta = \xi + i\eta = \operatorname{arccosh}\left(\frac{z}{c}\right) = \ln\left[\frac{z}{c} + \sqrt{\left(\frac{z}{c}\right)^2 - 1}\right] \tag{13}$$

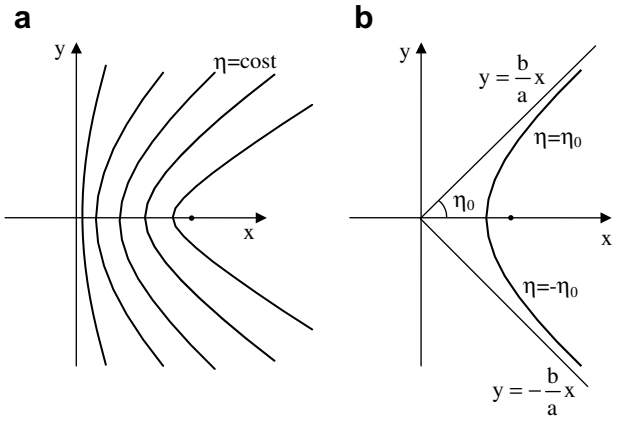

Fig. 2. Family of hyperbolae with the same foci (a); hyperbolic profile (1st and 4th quadrants) (b).

and so

$$\eta = \mathrm{Im}\left\{ \ln\left[\frac{z}{c} + \sqrt{\left(\frac{z}{c}\right)^2 - 1} \right] \right\}. \tag{14}$$

Remembering that (Lazzarin et al., 2007):

$$\ln\left[\frac{z}{c} + \sqrt{\left(\frac{z}{c}\right)^2 - 1} \right] = \ln\left| z + \sqrt{z^2 - c^2} \right| - \ln c + \mathrm{i}ph\left(\frac{z}{c} + \sqrt{\left(\frac{z}{c}\right)^2 - 1} \right) \tag{15}$$

and that

$$\sqrt{z^2 - c^2} = A\left(\cos\frac{\beta}{2} + \mathrm{i}\sin\frac{\beta}{2} \right), \tag{16}$$

being

$$A = \sqrt[4]{(x^2 - y^2 - c^2)^2 + 4x^2y^2} \tag{17}$$

and

$$\beta = \begin{cases} \arctan\left(\frac{2xy}{x^2 - y^2 - c^2}\right) & \text{if } x^2 - y^2 - c^2 > 0 \\ \arctan\left(\frac{2xy}{x^2 - y^2 - c^2}\right) + \pi & \text{if } x^2 - y^2 - c^2 < 0, \end{cases} \tag{18}$$

the following expressions immediately result:

$$\eta = \arctan\left(\frac{y + A\sin\frac{\beta}{2}}{x + A\cos\frac{\beta}{2}} \right), \tag{19}$$

$$\xi = \mathrm{arcsinh}\left(\frac{y}{c\sin\eta} \right). \tag{20}$$

Note that, if x and y are both positive, $0 \leqslant \xi < \infty$ and $0 < \eta \leqslant \frac{\pi}{2}$.

2.3. Hyperbolic–parabolic coordinate system

We shall also use an orthogonal curvilinear coordinate system generated by the transformation (Neuber, 1958; Lazzarin and Tovo, 1996):

$$z = w^q, \tag{21}$$

where $z = x + \mathrm{i}y$ and $w = u + \mathrm{i}v$ are complex variables in the physical and the transformed planes, respectively, and q is a real number related to the opening angle of the curve 2α:

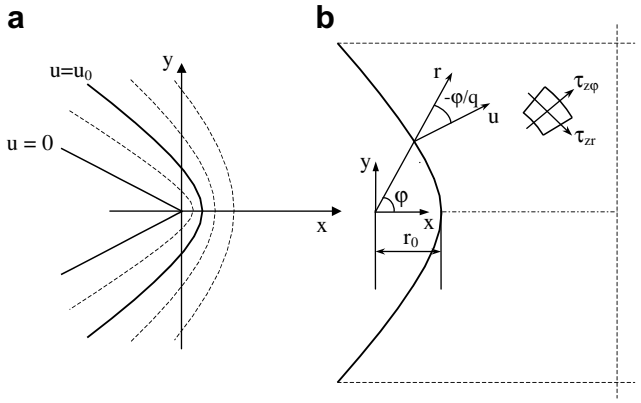

Fig. 3. (a) Auxiliary system of curvilinear coordinates (u,v); (b) reference system adopted for the solution.

$$q = \frac{2\pi - 2\alpha}{\pi} = \frac{2\gamma}{\pi}. \tag{22}$$

Eq. (21) can be re-written as:

$$w^q = (u + \mathrm{i}v)^q = \mathrm{re}^{\mathrm{i}\varphi} = r(\cos\varphi + \mathrm{i}\sin\varphi) \tag{23}$$

and so

$$\begin{cases} u = r^{\frac{1}{q}}\cos\frac{\varphi}{q} \\ v = r^{\frac{1}{q}}\sin\frac{\varphi}{q}. \end{cases} \tag{24}$$

The angle between the radial vector **r** and the normal vector **u** to the curve u = cost is then equal to $-\frac{\varphi}{q}$ (see Fig. 3b).

Moreover Eq. (24) results in:

$$r = (u^2 + v^2)^{\frac{q}{2}}. \tag{25}$$

The curvilinear coordinate system introduced here allows one to completely describe the hyperbolic ($1 < q < 2$) or parabolic ($q = 2$) profiles (see Fig. 3a). The generic curve characterised by the coordinate u_0 intersects the x-axis at a value:

$$r_0 = (u_0)^q. \tag{26}$$

So the parameter r_0 identifies the location of the reference system used with respect to the curve tip, and can be linked to the curvature radius by the following relationship:

$$\rho = \frac{qu_0^q}{(q-1)} = \frac{qr_0}{(q-1)}. \tag{27}$$

The value $q = 1$ represents a semi-infinite plane (smooth shaft).

3. A first class of solutions by using the hyperbolic transformation

3.1. General formulation of the problem

The circumferential hyperbolic notch problem in an infinite shaft has to be treated by noting that the nominal shear stress on the gross section must fall to zero to preserve a finite stress across the net waist.

The complex potential that inherently respects this assumption is:

$$H(z) = Ac\zeta, \tag{28}$$

where $A = A_1 + \mathrm{i}A_2$ is a complex coefficient and $\zeta = \xi + \mathrm{i}\eta$ is the transformed variable.

Note that it coincides with one of the two potentials already used by Timoshenko and Goodier (1970) to solve the plane problem of a double-symmetric-hyperbolic notch in a plate under tension.

According to Eq. (6) $\frac{\partial z}{\partial \zeta} = c\sinh\zeta$, and by means of Eq. (1):

$$H'(z) = \frac{\partial H(z)}{\partial \zeta}\cdot\frac{\partial \zeta}{\partial z} = \frac{(A_1 + \mathrm{i}A_2)}{\sinh\zeta} = \tau_{zx} - \mathrm{i}\tau_{zy}, \tag{29}$$

The hyperbolic transformation allows one to completely describe the notch profile by means of the curve $\eta = \eta_0$ (in the first quadrant).

Noting that

$$\begin{aligned}\frac{1}{\sinh\zeta} &= \frac{1}{\frac{e^{\xi+i\eta}-e^{-\xi-i\eta}}{2}} = \frac{1}{\frac{e^{\xi}}{2}(\cos\eta+i\sin\eta)-\frac{e^{-\xi}}{2}(\cos\eta-i\sin\eta)} \\ &= \frac{\cos\eta\sinh\xi - i\sin\eta\cosh\xi}{\cos^2\eta\sinh^2\xi+\sin^2\eta\cosh^2\xi} = \frac{2\cos\eta\sinh\xi-2i\sin\eta\cosh\xi}{\cosh 2\xi-\cos 2\eta},\end{aligned} \tag{30}$$

the function $H'(z)$ can be re-written as follows:

$$\begin{aligned}H'(z) &= \frac{(A_1+iA_2)}{\sinh\zeta} = (A_1+iA_2)\frac{2\cos\eta\sinh\xi-2i\sin\eta\cosh\xi}{\cosh 2\xi-\cos 2\eta} \\ &= \left(\frac{2A_1\cos\eta\sinh\xi+2A_2\sin\eta\cosh\xi}{\cosh 2\xi-\cos 2\eta}\right)+i\left(\frac{2A_2\cos\eta\sinh\xi-2A_1\sin\eta\cosh\xi}{\cosh 2\xi-\cos 2\eta}\right).\end{aligned} \tag{31}$$

So

$$\begin{aligned}\tau_{zx} &= \frac{2A_1\cos\eta\sinh\xi+2A_2\sin\eta\cosh\xi}{\cosh 2\xi-\cos 2\eta}, \\ \tau_{zy} &= -\frac{2A_2\cos\eta\sinh\xi-2A_1\sin\eta\cosh\xi}{\cosh 2\xi-\cos 2\eta}.\end{aligned} \tag{32}$$

Observing that

$$\begin{aligned}&\tau_{z\eta}|_{\eta=\eta_0} = 0;\ \text{being}\ \tau_{z\eta}|_{\substack{\eta=\eta_0\\ \xi=0}} = \tau_{zx}, \\ &\tau_{zx}|_{\substack{\eta=\eta_0\\ \xi=0}} = \frac{2A_2\sin\eta_0}{1-\cos 2\eta_0} = 0 \rightarrow A_2 = 0,\end{aligned} \tag{33}$$

and stresses can be written as a function of the parameter A_1 which can be determined as a function of the external loading conditions:

$$\begin{aligned}\tau_{zx} &= \frac{2A_1\cos\eta\sinh\xi}{\cosh 2\xi-\cos 2\eta}, \\ \tau_{zy} &= \frac{2A_1\sin\eta\cosh\xi}{\cosh 2\xi-\cos 2\eta}.\end{aligned} \tag{34}$$

It is possible to note that when $\xi = 0$

$$\cos\eta = \frac{x}{c}, \tag{35}$$

$$\sin\eta = \sqrt{1-\frac{x^2}{c^2}}, \tag{36}$$

and

$$\cos 2\eta = \cos^2\eta - \sin^2\eta = \frac{2x^2}{c^2} - 1. \tag{37}$$

$$\tau_{zy}|_{\xi=0} = \frac{2A_1\sin\eta}{1-\cos 2\eta} = \frac{2A_1\sqrt{1-\frac{x^2}{c^2}}}{2\left(1-\frac{x^2}{c^2}\right)} = \frac{cA_1}{\sqrt{c^2-x^2}} \tag{38}$$

and, at the notch tip:

$$\tau_{\max} = \frac{cA_1}{\sqrt{c^2-a^2}}. \tag{39}$$

Furthermore, as $\rho = \frac{b^2}{a}$ (Neuber, 1958), the following relationships are valid:

$$\frac{a^2}{b^2} = \frac{a}{\rho} \quad \text{and} \quad c = \sqrt{a^2+b^2} = b\sqrt{\frac{a^2}{b^2}+1} = b\sqrt{\frac{a}{\rho}+1} \tag{40}$$

and so

$$A_1 = \tau^*\frac{b}{c}K_{t,net} = \tau^*\frac{K_{t,net}}{\sqrt{1+\frac{a}{\rho}}}. \tag{41}$$

Stresses can be re-written as a function of the stress concentration factor, obviously referred to the net section:

$$\tau_{zx} = \tau^* \frac{2K_{t,net}}{\sqrt{1+\frac{a}{\rho}}} \frac{\cos\eta \sinh\xi}{\cosh 2\xi - \cos 2\eta},$$
$$\tau_{zy} = \tau^* \frac{2K_{t,net}}{\sqrt{1+\frac{a}{\rho}}} \frac{\sin\eta \cosh\xi}{\cosh 2\xi - \cos 2\eta}. \tag{42}$$

Shear strain components can be determined as:

$$\gamma_{zx} = \frac{\tau_{zx}}{G} = \tau^* \frac{2K_{t,net}}{G\sqrt{1+\frac{a}{\rho}}} \frac{\cos\eta \sinh\xi}{\cosh 2\xi - \cos 2\eta},$$
$$\gamma_{zy} = \frac{\tau_{zy}}{G} = \tau^* \frac{2K_{t,net}}{G\sqrt{1+\frac{a}{\rho}}} \frac{\sin\eta \cosh\xi}{\cosh 2\xi - \cos 2\eta}. \tag{43}$$

Furthermore, Eq. (5) gives:

$$w = \frac{\mathrm{Re}\{H(z)\}}{G} = \tau^* \frac{cK_{t,net}\xi}{G\sqrt{1+\frac{a}{\rho}}}. \tag{44}$$

It must be observed that the obtained solutions are valid for a uniform antiplane shear loading. In the case of torsion loading it is necessary to take into account the linear decrease of the nominal shear stress. This can be done, by means of some simple geometrical considerations, see Fig. 4, introducing in Eqs. (42) the following correction factor:

$$\frac{x^*}{x_{edge}}, \tag{45}$$

where x^* is the x-coordinate of the point P in which stresses are going to be evaluated, whilst x_{edge} is the x-coordinate of the point on the notch edge having the same value of the y-coordinate.

Calling (x^*,y^*) the Cartesian coordinates of the generic point P:

$$x_{edge} = c\cos\eta_0 \cosh\xi^*, \tag{46}$$

where

$$\xi^* = \mathrm{arcsinh}\left(\frac{y^*}{c\sin\eta_0}\right). \tag{47}$$

So

$$\frac{x^*}{x_{edge}} = \frac{c\cos\eta\cosh\xi}{c\cos\eta_0\cosh\xi^*}. \tag{48}$$

Along the notch bisector we have $\xi = 0$, and Eq. (48) immediately gives:

$$\frac{x^*}{x_{edge}} = \frac{c\cos\eta\cosh 0}{c\cos\eta_0\cosh 0} = \frac{x}{a}. \tag{49}$$

Taking into account the linear decrease effect, stress components are:

$$\tau_{zx} = \tau^* \frac{2K_{t,net}}{\sqrt{1+\frac{a}{\rho}}} \cdot \frac{\cos\eta\sinh\xi}{\cosh 2\xi - \cos 2\eta} \cdot \frac{\cos\eta\cosh\xi}{\cos\eta_0\cosh\xi^*},$$
$$\tau_{zy} = \tau^* \frac{2K_{t,net}}{\sqrt{1+\frac{a}{\rho}}} \cdot \frac{\sin\eta\cosh\xi}{\cosh 2\xi - \cos 2\eta} \cdot \frac{\cos\eta\cosh\xi}{\cos\eta_0\cosh\xi^*}, \tag{50}$$

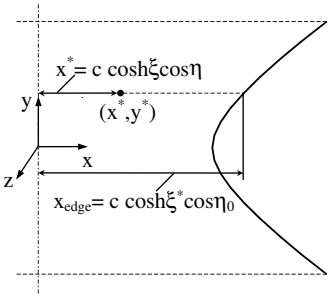

Fig. 4. Geometrical relationships to determine the correction factor taking into account the linear decrease of the nominal shear stress (hyperbolic transformation).

that is

$$\tau_{zx} = \tau^* \frac{K_{t,net}}{\sqrt{1+\frac{a}{\rho}}} \cdot \frac{\cos^2\eta \sinh 2\xi}{\cos\eta_0 \cosh\xi^* (\cosh 2\xi - \cos 2\eta)},$$
$$\tau_{zy} = \tau^* \frac{K_{t,net}}{\sqrt{1+\frac{a}{\rho}}} \cdot \frac{\sin 2\eta \cosh^2\xi}{\cos\eta_0 \cosh\xi^* (\cosh 2\xi - \cos 2\eta)}. \quad (51)$$

3.2. Evaluation of the stress concentration factor in the case of torsion loading

On the net section the nominal stress τ and the notch-affected stress τ_{zy} must be in equilibrium. Both of them are influenced by the linear decrease effect of Coulomb distribution. The equilibrium condition on the net section is:

$$\int_A \tau(x) x \, dA = \int_A \tau_{zy} x \, dA, \quad (52)$$
$$\int_0^{2\pi} \int_0^a \tau(x) x^2 \, dx \, d\theta = \int_0^{2\pi} \int_0^a \tau_{zy} x^2 \, dx \, d\theta, \quad (53)$$

where

$$\tau(x) = \tau^* \frac{x}{a} \quad (54)$$

and

$$\tau_{zy}|_{\xi=0} = \tau^* \frac{2K_{t,\,net}}{\sqrt{1+\frac{a}{\rho}}} \cdot \frac{\sin\eta\cosh\xi}{\cosh 2\xi - \cos 2\eta} \cdot \frac{\cos\eta\cosh\xi}{\cos\eta_0\cosh\xi^*} = \frac{\tau^* b K_{t,net}}{\sqrt{c^2-x^2}} \cdot \frac{x}{a}. \quad (55)$$

So

$$\frac{2\pi}{a}\frac{a^4\tau^*}{4} = 2\pi\tau^* \frac{bK_{t,net}}{a} \int_0^a \frac{x^3}{\sqrt{c^2-x^2}} \, dx \quad (56)$$

that is

$$K_{t,net} = \frac{3}{4} \cdot \frac{a^4}{2bc^3 - b^2(a^2+2c^2)}. \quad (57)$$

Remembering relations (40), Eq. (57) can be re-written as:

$$K_{t,net} = \frac{3}{4} \cdot \frac{a^4}{2b^4\sqrt{\frac{a}{\rho}+1} \cdot \left(\frac{a}{\rho}+1\right) - b^4\left[\frac{a}{\rho}+2\left(\frac{a}{\rho}+1\right)\right]} \quad (58)$$

that is

$$K_{t,net} = \frac{3}{4} \frac{\left(\frac{a}{\rho}\right)^2}{2\left(\frac{a}{\rho}+1\right) \cdot \left(\sqrt{\frac{a}{\rho}+1}-1\right) - \frac{a}{\rho}}. \quad (59)$$

This result agrees with that by Neuber (1958) for a deep notch, even if written in a different form:

$$K_{t,net,Neuber} = \frac{3}{4} \frac{\left(1+\sqrt{\frac{a}{\rho}+1}\right)^2}{\left(1+2\sqrt{\frac{a}{\rho}+1}\right)}. \quad (60)$$

Stresses can also be written explicitly by substituting the stress concentration factor:

$$\tau_{zx} = \frac{3\tau^*}{4\sqrt{1+\frac{a}{\rho}}} \cdot \frac{\left(\frac{a}{\rho}\right)^2}{2\left(\frac{a}{\rho}+1\right) \cdot \left(\sqrt{\frac{a}{\rho}+1}-1\right) - \frac{a}{\rho}} \cdot \frac{\cos^2\eta\sinh 2\xi}{\cos\eta_0\cosh\xi^*(\cosh 2\xi - \cos 2\eta)},$$
$$\tau_{zy} = \frac{3\tau^*}{4\sqrt{1+\frac{a}{\rho}}} \cdot \frac{\left(\frac{a}{\rho}\right)^2}{2\left(\frac{a}{\rho}+1\right) \cdot \left(\sqrt{\frac{a}{\rho}+1}-1\right) - \frac{a}{\rho}} \cdot \frac{\sin 2\eta\cosh^2\xi}{\cos\eta_0\cosh\xi^*(\cosh 2\xi - \cos 2\eta)}. \quad (61)$$

3.3. Evaluation of the stress concentration factor in the case of uniform antiplane shear

In the same way, it is possible to determine the stress concentration factor for uniform antiplane shear. In this case stresses do not decrease linearly and the stress concentration factor becomes:

$$K_{t,net} = \frac{a^3}{3b}\frac{1}{\int_0^a \frac{x^2}{\sqrt{c^2-x^2}}\,dx} = \frac{2}{3}\frac{a^3}{bc^2\arcsin\left(\frac{a}{c}\right) - ba\sqrt{c^2-a^2}} = \frac{2}{3}\frac{a^3}{b^3\frac{c^2}{b^2}\arcsin\left(\frac{a}{c}\right) - b^3\frac{a}{b}} = \frac{2}{3}\frac{a^3}{b^3}\frac{1}{\frac{c^2}{b^2}\arcsin\left(\frac{a}{c}\right) - \frac{a}{b}} \tag{62}$$

Furthermore, by means of relations (40):

$$K_{t,net} = \frac{2}{3}\frac{\left(\frac{a}{\rho}\right)^{\frac{3}{2}}}{\left(1+\frac{a}{\rho}\right)\arcsin\left(\frac{\sqrt{\frac{a}{\rho}}}{\sqrt{1+\frac{a}{\rho}}}\right) - \sqrt{\frac{a}{\rho}}}. \tag{63}$$

3.4. A comparison with numerical results

Figs. 5–8 show a comparison between the results obtained by a number of elastic finite element analyses on notched shafts of different dimension and those given by Eq. (61). The agreement is good even in the case of finite items, at least when stresses are evaluated along the notch bisector line.

4. A second class of solutions by using the hyperbolic–parabolic transformation

4.1. General formulation of the problem

We shall use the same form for the function $H(z)$ already used in the former case:

$$H(z) = Aw, \tag{64}$$

where $A = A_1 + iA_2$ is a complex coefficient and $w = u + iv$ is the transformed variable.

So, remembering that $\frac{\partial z}{\partial w} = qw^{q-1}$ and using Eq. (1):

$$H'(z) = \frac{\partial H(z)}{\partial w}\cdot\frac{\partial w}{\partial z} = \frac{(A_1 + iA_2)}{qw^{q-1}} = \tau_{zx} - i\tau_{zy}. \tag{65}$$

The adopted transformation allows one to completely describe a hyperbolic or parabolic profile by means of the curve $u = u_0$. It is also possible to re-write the function $H'(z)$ as:

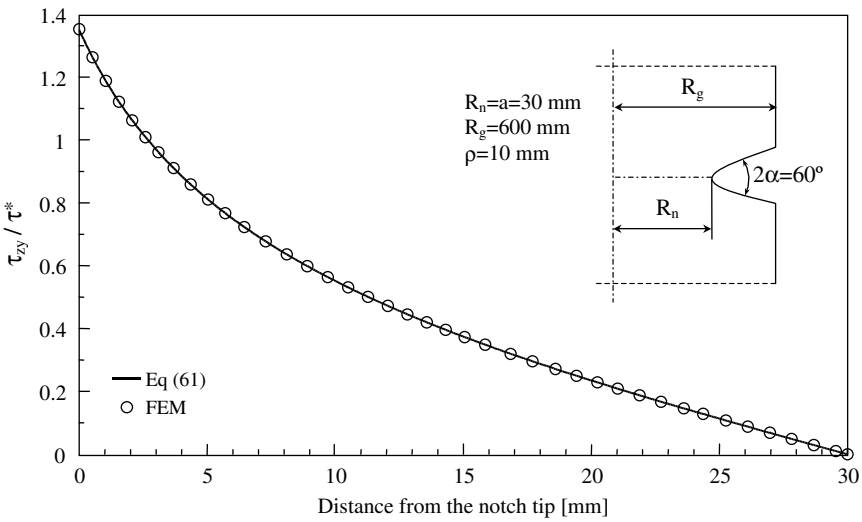

Fig. 5. Plot of the stress component τ_{zy} along the notch bisector line. The stress component is normalised with respect to the maximum value of the nominal stress on the net area (hyperbolic notch).

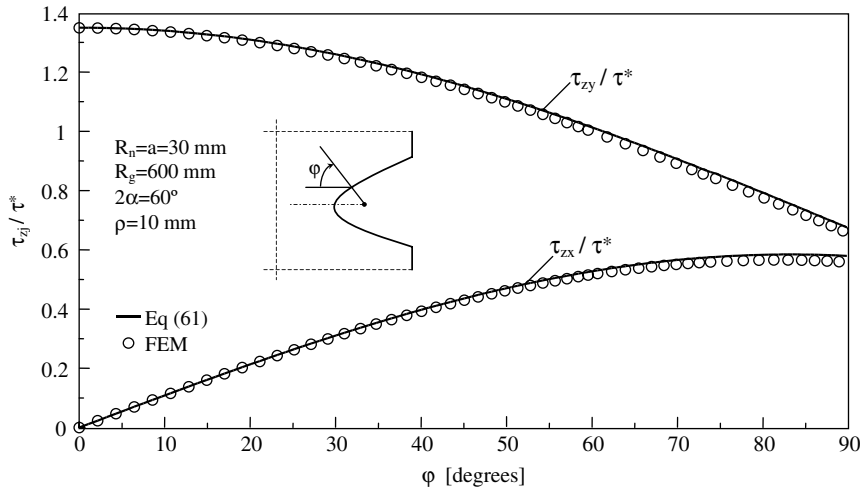

Fig. 6. Stress fields plotted along the notch edge; stresses normalised with respect to the maximum value of the nominal stress on the net area. The parameter φ represents the angle between the x-direction and the line connecting the notch focus and the point at which stresses are evaluated (hyperbolic notch).

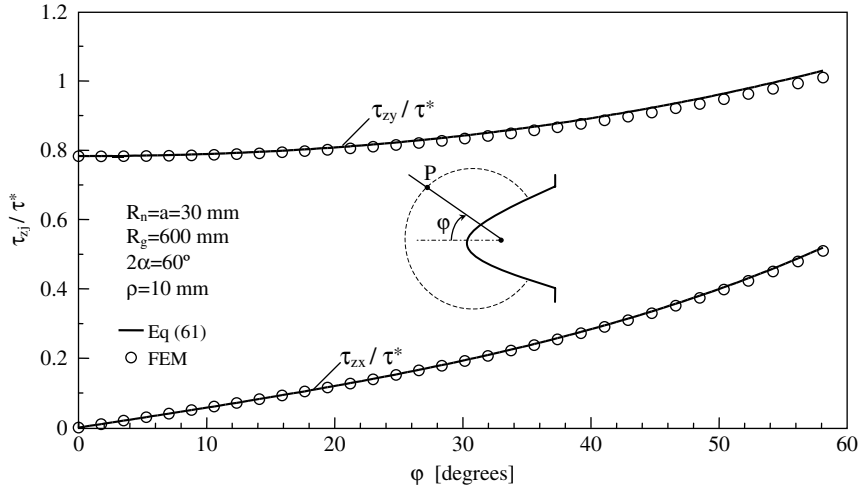

Fig. 7. Stress fields plotted along a circular path of radius equal to 5.5 mm and centred on the notch tip; stresses normalised with respect to the maximum value of the nominal stress on the net area. The parameter φ represents the angle between the x-direction and the line connecting the notch focus and the point at which stresses are evaluated (hyperbolic notch).

$$H'(z) = \frac{(A_1 + \mathrm{i}A_2)}{q(u + \mathrm{i}v)^{q-1}} = \frac{(A_1 + \mathrm{i}A_2)(u - \mathrm{i}v)^{q-1}}{q(u^2 + v^2)^{q-1}}. \tag{66}$$

At the notch tip, when $v = 0$ and $u = u_0$

$$H'(z)|_{\substack{v=0 \\ u=u_0}} = \frac{(A_1 + \mathrm{i}A_2)u_0^{q-1}}{qu_0^{2(q-1)}} = \frac{A_1 + \mathrm{i}A_2}{qu_0^{q-1}} \tag{67}$$

and, being

$$\tau_{zx}|_{\substack{u=u_0 \\ v=0}} = \frac{A_1}{qu_0^{q-1}} = 0 \rightarrow A_1 = 0, \tag{68}$$

one can write

$$H'(z) = \frac{\mathrm{i}A_2(u - \mathrm{i}v)^{q-1}}{q(u^2 + v^2)^{q-1}}. \tag{69}$$

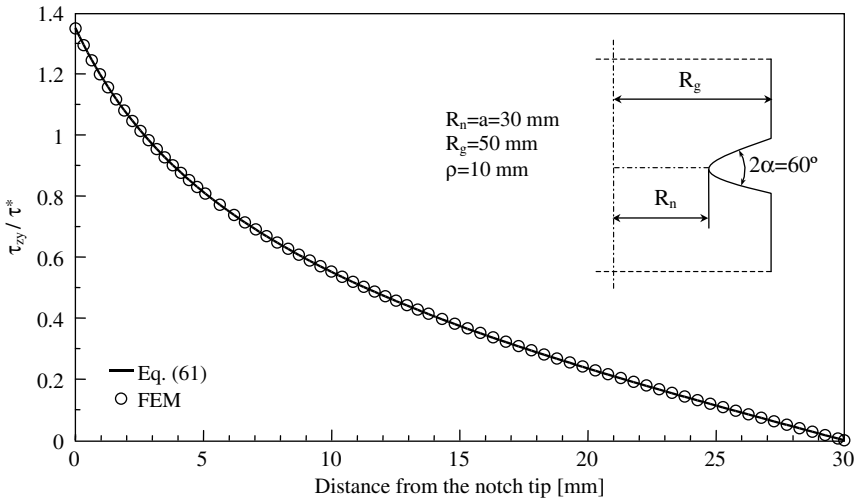

Fig. 8. Plot of the stress component τ_{zy} along the notch bisector. The stress component is normalised with respect to the maximum value of the nominal stress on the net area (hyperbolic notch).

Now remembering Eqs. (24) and (25) and Euler's formula:

$$H'(z)=\frac{iA_2(u-iv)^{q-1}}{q(u^2+v^2)^{q-1}}=\frac{iA_2}{qr^{\frac{2(q-1)}{q}}}r^{\frac{q-1}{q}}\left(\cos\frac{\varphi}{q}-i\sin\frac{\varphi}{q}\right)^{q-1}=\frac{iA_2}{qr^{\frac{q-1}{q}}}\left[\cos\left(\frac{q-1}{q}\varphi\right)-i\sin\left(\frac{q-1}{q}\varphi\right)\right]. \tag{70}$$

Stress components are defined in terms of an unknown constant, A_2, which can be determined as a function of the external loading conditions:

$$\begin{aligned}\tau_{zx}&=\frac{A_2}{qr^{\frac{q-1}{q}}}\sin\left(\frac{q-1}{q}\varphi\right),\\ \tau_{zy}&=\frac{-A_2}{qr^{\frac{q-1}{q}}}\cos\left(\frac{q-1}{q}\varphi\right).\end{aligned} \tag{71}$$

Note that, when $\varphi=0$, Eq. (71) coincides with the expression for τ_{zy} stress components obtained in a different way by Neuber (1958) along the bisector line of a 'pointed notch' under longitudinal shear.

In terms of polar coordinates:

$$\begin{Bmatrix}\tau_{zr}\\ \tau_{z\varphi}\end{Bmatrix}=\begin{bmatrix}\cos\varphi & \sin\varphi\\ -\sin\varphi & \cos\varphi\end{bmatrix}\begin{Bmatrix}\tau_{zx}\\ \tau_{zy}\end{Bmatrix} \tag{72}$$

and so

$$\begin{aligned}\tau_{zr}&=\frac{-A_2}{qr^{\frac{q-1}{q}}}\sin\left(\frac{1}{q}\varphi\right),\\ \tau_{z\varphi}&=\frac{-A_2}{qr^{\frac{q-1}{q}}}\cos\left(\frac{1}{q}\varphi\right).\end{aligned} \tag{73}$$

4.2. An alternative formulation of the problem

The same solution can be obtained using for $H(z)$ the following form:

$$H(z)=Az^{\lambda} \tag{74}$$

and so

$$H'(z)=(A_1+iA_2)\lambda z^{\lambda-1}, \tag{75}$$

being λ a real number and A a complex coefficient. Note that the function $H(z)$ coincides with the first potential already used to solve the plane problem of an infinite notched plate (England, 1971; Lazzarin and Tovo, 1996).

Consider a polar reference system centred at the focus of the notch profile at a distance r_0 from the notch tip, along the notch bisector (see Fig. 3b). It is possible to write:

$$\begin{aligned} e^{i\varphi}H'(z) &= e^{i\varphi}(A_1 + iA_2)\lambda r^{\lambda-1}e^{i(\lambda-1)\varphi} = [(A_1 + iA_2)\lambda r^{\lambda-1}](\cos\lambda\varphi + i\sin\lambda\varphi) \\ &= \lambda r^{\lambda-1}[(A_1\cos\lambda\varphi - A_2\sin\lambda\varphi) + i(A_1\sin\lambda\varphi + A_2\cos\lambda\varphi)] \end{aligned} \tag{76}$$

and

$$\begin{aligned} \tau_{zr} &= \mathrm{Re}\{e^{i\varphi}H'(z)\} = \lambda r^{\lambda-1}(-A_2\sin\lambda\varphi + A_1\cos\lambda\varphi), \\ \tau_{z\varphi} &= -\mathrm{Im}\{e^{i\varphi}H'(z)\} = \lambda r^{\lambda-1}(-A_1\sin\lambda\varphi - A_2\cos\lambda\varphi). \end{aligned} \tag{77}$$

The coefficients A_i can be determined by imposing boundary conditions on the notch edge characterised by the curve $u = u_0$:

$$(\tau_{zu})_{u=u_0} = 0. \tag{78}$$

To simplifying the mathematical analysis it is useful to impose the condition at infinity:

$$(\tau_{zu})_{\substack{u=u_0 \\ v\gg 0}} = 0. \tag{79}$$

At $r \to \infty$ the conic defined by $u = u_0$ presents the same inclination of the flanks of the V-notch with the same opening angle, which, from a mathematical point of view, represent the two asymptotes; so Eq. (79) can be re-written in polar coordinates as:

$$\lim_{\substack{r\to+\infty \\ \varphi\to\pm\gamma}} (r^{1-\lambda}\tau_{z\varphi}) = 0, \tag{80}$$

giving the following system:

$$\begin{bmatrix} \sin\lambda\gamma & \cos\lambda\gamma \\ -\sin\lambda\gamma & \cos\lambda\gamma \end{bmatrix} \begin{Bmatrix} A_1 \\ A_2 \end{Bmatrix} = \underline{0}. \tag{81}$$

Rouchè–Capelli's condition provides the characteristic equation of the system, whose roots represent the eigenvalues of the problem:

$$2\sin\lambda\gamma\cos\lambda\gamma = \sin 2\lambda\gamma = 0. \tag{82}$$

Eq. (82) has, in general, an infinite number of solutions, but we are interested only in the smaller positive value of λ_3 that is:

$$\lambda_3 = \frac{\pi}{2\gamma} = \frac{1}{q}. \tag{83}$$

Thus, the first equation of the system results in:

$$A_1 = -A_2 \cdot \frac{\cos\lambda_3\gamma}{\sin\lambda_3\gamma} = -A_2 \cdot \frac{\cos(\pi/2)}{\sin(\pi/2)} = 0. \tag{84}$$

Finally, we can re-write Eq. (77), providing shear stress components:

$$\begin{Bmatrix} \tau_{zr} \\ \tau_{z\varphi} \end{Bmatrix} = -\lambda_3 r^{\lambda_3-1} A_2 \begin{Bmatrix} \sin\lambda_3\varphi \\ \cos\lambda_3\varphi \end{Bmatrix}, \tag{85}$$

which coincides with the previous solution given by Eq. (73).

Indeed considering Eq. (21), Eq. (74) can be re-written as:

$$H(z) = Az^{\lambda} = Aw^{\lambda q} \tag{86}$$

and as $\lambda_3 = 1/q$, Eq. (84) immediately matches Eq. (64).

Shear strain components can be determined as:

$$\begin{Bmatrix} \gamma_{zr} \\ \gamma_{z\varphi} \end{Bmatrix} = \begin{Bmatrix} \frac{\tau_{zr}}{G} \\ \frac{\tau_{z\varphi}}{G} \end{Bmatrix} = \frac{-\lambda_3 r^{\lambda_3-1} A_2}{G} \begin{Bmatrix} \sin\lambda_3\varphi \\ \cos\lambda_3\varphi \end{Bmatrix}. \tag{87}$$

Moreover Eq. (5) gives:

$$Gw = \mathrm{Re}\{H(z)\}. \tag{88}$$

Having chosen $H(z) = A\,z^{\lambda}$ and remembering that $A_1 = 0$:

$$\frac{\mathrm{Re}\{H(z)\}}{G} = w = -\frac{A_2 r^{\lambda_3}}{G}\sin\lambda_3\varphi. \tag{89}$$

Stress, strain and displacement fields are defined in terms of an unknown constant, A_2, which can be determined as a function of the external loading conditions. Note also that no hypothesis or limitation has been made about the value of the notch

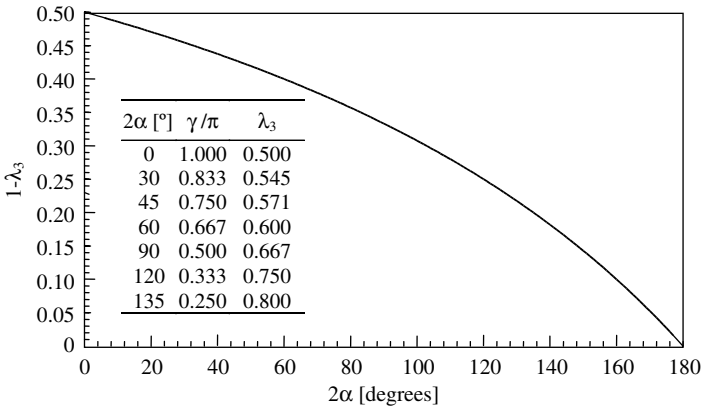

Fig. 9. Eigenvalue λ_3 as a function of the notch-opening angle 2α.

root radius or the opening angle; the obtained solution can be considered as general and useful to describe different types of notches. Fig. 9 shows the value of $1-\lambda_3$ as a function of the notch-opening angle.

4.3. Stress, strain and displacement fields as a function of a field parameter

Modes I and II N-SIF definitions for blunt V-notches were given by Lazzarin and Tovo (1996) and by Atzori et al. (1997) by extending those proposed by Gross and Mendelson for sharp V-notches (Gross and Mendelson, 1972). Subsequently the analytical frame was improved by Filippi et al. (2002) by adding a complex potential to the stress analytical functions.

Filippi's solution was revisited by Dini and Hills (2004, 2006) who proposed a general procedure for quantifying the singular stress field at the tip of a notionally sharp notch, but possessing a small root radius, by using in combination Williams' solution for the semi-infinite sharp V-notch and Filippi's solution for the semi-infinite rounded notch (Williams, 1952; Filippi et al., 2002), all stresses being written by Dini and Hills as a function of the relevant Mode I N-SIFs. Some closed-form expressions linking the Mode I N-SIFs from sharp and blunt V-notches were given by Lazzarin and Filippi (2006), whereas the link between the *J*-integral (Rice, 1968) and the strain energy in a given, material-dependent, finite size volume surrounding the notch tip was underlined by Berto and Lazzarin (2007).

Extending the N-SIF definitions from the plane problems to the antiplane case gives:

$$K_{3\rho} = \sqrt{2\pi} \lim_{r \to r_0^+} [r^{1-\lambda_3} \tau_{z\varphi}(r, \varphi = 0)]. \tag{90}$$

Substituting Eq. (85) into Eq. (90) and using limit properties:

$$A_2 = -\frac{K_{3\rho}}{\sqrt{2\pi}\lambda_3} \tag{91}$$

and so

$$\begin{Bmatrix} \tau_{zr}(r,\varphi) \\ \tau_{z\varphi}(r,\varphi) \end{Bmatrix} = \frac{K_{3\rho} r^{\lambda_3 - 1}}{\sqrt{2\pi}} \begin{Bmatrix} \sin\lambda_3\varphi \\ \cos\lambda_3\varphi \end{Bmatrix}, \tag{92}$$

$$\begin{Bmatrix} \gamma_{zr}(r,\varphi) \\ \gamma_{z\varphi}(r,\varphi) \end{Bmatrix} = \frac{K_{3\rho} r^{\lambda_3 - 1}}{G\sqrt{2\pi}} \begin{Bmatrix} \sin\lambda_3\varphi \\ \cos\lambda_3\varphi \end{Bmatrix}, \tag{93}$$

$$w = \frac{K_{3\rho}}{G\sqrt{2\pi}\lambda_3} r^{\lambda_3} \sin\lambda_3\varphi. \tag{94}$$

4.4. Stress, strain and displacement fields as a function of the maximum shear stress

When the notch root radius is not zero, or not too small, the coefficient A_2 can be determined as a function of the maximum shear stress occurring at the notch tip:

$$A_2 = \frac{-\tau_{\max}}{\lambda_3 r_0^{\lambda_3 - 1}} \tag{95}$$

and so

$$\left\{ \begin{array}{l} \tau_{zr}(r,\varphi) \\ \tau_{z\varphi}(r,\varphi) \end{array} \right\} = \tau_{\max} \left(\frac{r}{r_0}\right)^{\lambda_3 - 1} \left\{ \begin{array}{l} \sin \lambda_3 \varphi \\ \cos \lambda_3 \varphi \end{array} \right\}, \tag{96}$$

$$\left\{ \begin{array}{l} \gamma_{zr}(r,\varphi) \\ \gamma_{z\varphi}(r,\varphi) \end{array} \right\} = \frac{\tau_{\max}}{G} \left(\frac{r}{r_0}\right)^{\lambda_3 - 1} \left\{ \begin{array}{l} \sin \lambda_3 \varphi \\ \cos \lambda_3 \varphi \end{array} \right\}, \tag{97}$$

$$w = \frac{\tau_{\max}}{G} \frac{r_0}{\lambda_3} \left(\frac{r}{r_0}\right)^{\lambda_3} \sin \lambda_3 \varphi. \tag{98}$$

Note that, equating Eqs. (91) and (95) results in the following relationship between the generalised stress intensity factor and the maximum shear stress:

$$K_{3\rho} = \tau_{\max} \sqrt{2\pi} r_0^{1-\lambda_3}. \tag{99}$$

4.5. Solution for some special profiles

4.5.1. The crack case

The case $2\alpha = 0^\circ$ and $\rho = 0$ mm represents a circumferential edge crack. As $q = 2$

$$\lambda_3 = 1/q = 0.5,$$

and, substituting K_3 with K_{III}, Eq. (92) matches the well-known equations of LEFM:

$$\left\{ \begin{array}{l} \tau_{zr}(r,\varphi) \\ \tau_{z\varphi}(r,\varphi) \end{array} \right\} = \frac{K_{III}}{\sqrt{2\pi r}} \left\{ \begin{array}{l} \sin \frac{1}{2}\varphi \\ \cos \frac{1}{2}\varphi \end{array} \right\}. \tag{100}$$

Recently Lazzarin et al. (2007) obtained the same result starting from a degenerating-to-crack semi-ellipse and considering only the first term of an asymptotic expansion.

4.5.2. The parabolic notch

The case $2\alpha = 0^\circ$ and $\rho \neq 0$ represents a parabolic notch. With $2\alpha = \pi(2 - q)$:

$$\lambda_3 = 1/q = 0.5.$$

Stress fields can be equivalently written as a function of the generalised N-SIF:

$$\left\{ \begin{array}{l} \tau_{zr}(r,\varphi) \\ \tau_{z\varphi}(r,\varphi) \end{array} \right\} = \frac{K_{3\rho}}{\sqrt{2\pi r}} \left\{ \begin{array}{l} \sin \frac{1}{2}\varphi \\ \cos \frac{1}{2}\varphi \end{array} \right\}, \tag{101}$$

or as a function of the maximum shear stress:

$$\left\{ \begin{array}{l} \tau_{zr}(r,\varphi) \\ \tau_{z\varphi}(r,\varphi) \end{array} \right\} = \tau_{\max} \left(\frac{\rho}{2r}\right)^{0.5} \left\{ \begin{array}{l} \sin \frac{1}{2}\varphi \\ \cos \frac{1}{2}\varphi \end{array} \right\}. \tag{102}$$

Eq. (101) coincide with those of Creager and Paris for *blunt cracks* (Creager and Paris, 1967).

Further, from Eq. (99), substituting the appropriate values of the parameters involved, one can obtain:

$$K_{3\rho} = \tau_{\max} \sqrt{\pi\rho}, \tag{103}$$

which coincides with that proposed by Hasebe and Kutanda (1978).

Note also that, for an infinite shaft weakened by a circumferential semi-elliptic notch, the maximum shear stress occurring at the notch tip is (Neuber, 1958; Lazzarin et al., 2007):

$$\tau_{\max} = \left(1 + \frac{a}{b}\right)\tau. \tag{104}$$

Substituting Eq. (104) into Eq. (103) and ρ tending to zero, one obtains the Mode III SIF for a circumferential edge crack in an infinite shaft:

$$K_{III} = \lim_{\rho \to 0} (\tau_{\max} \sqrt{\pi\rho}) = \tau \lim_{\rho \to 0} \left(\left(1 + \sqrt{\frac{a}{\rho}}\right) \sqrt{\pi\rho} \right) = \tau \sqrt{\pi a}. \tag{105}$$

This relation has already been obtained by Lazzarin et al. (2007) starting from stress distributions resulting from a degenerating-to-crack semi-elliptic circumferential notch and applying the following definition:

$$K_{III} = \lim_{x \to a} \sqrt{2\pi(x - a)} \tau_{zy}|_{y=0}. \tag{106}$$

So, even for a semi-elliptic circumferential notch, Eq. (103) has to be thought of as valid when the notch root radius is small compared to the notch depth; this happens because in such a situation stress distributions for a semi-elliptic notch asymptotically tends to those valid for a parabolic notch (see Appendix A).

4.5.3. The sharp V-notch

When $\rho = 0$ the notch is a sharp V-notch and Eqs. (83), (85) and (87), become those reported in the literature (Seweryn and Molski, 1996; Qian and Hasebe, 1997; Dunn et al., 1997).

Stresses can be written in terms of the field parameter K_3:

$$\left\{ \begin{array}{l} \tau_{zr}(r,\varphi) \\ \tau_{z\varphi}(r,\varphi) \end{array} \right\} = \frac{K_3 r^{\lambda_3 - 1}}{\sqrt{2\pi}} \left\{ \begin{array}{l} \sin\lambda_3\varphi \\ \cos\lambda_3\varphi \end{array} \right\}. \tag{107}$$

4.6. The correction of stress distributions to take into account the linear decrease of the nominal shear stress

The solutions obtained are valid for uniform antiplane shear loading. For torsion loading it is necessary to take into account the linear decrease of the nominal shear stress. This can be done in two different ways for a sharp V-notch or a rounded notch.

4.6.1. Sharp V-notches

The linear decrease of the nominal shear stress can be taken into account by means of some simple geometrical considerations, see Fig. 10a, correcting Eq. (92) in the following way:

$$\left\{ \begin{array}{l} \tau_{zr}(r,\varphi) \\ \tau_{z\varphi}(r,\varphi) \end{array} \right\} = \frac{K_3 r^{\lambda_3 - 1}}{\sqrt{2\pi}} \left\{ \begin{array}{l} \sin\lambda_3\varphi \\ \cos\lambda_3\varphi \end{array} \right\} \left(1 - \frac{\frac{r\sin\varphi}{\tan\alpha} + r\cos\varphi}{R + \frac{r\sin\varphi}{\tan\alpha}} \right), \quad \alpha \neq 0. \tag{108}$$

R being the radius of the net section of the shaft.

4.6.2. Parabolic and hyperbolic notches

The linear decrease of the nominal shear stress can be taken into account by means of some simple geometrical considerations, see Fig. 10b, correcting Eq. (96) in the following way:

$$\left\{ \begin{array}{l} \tau_{zr}(r,\varphi) \\ \tau_{z\varphi}(r,\varphi) \end{array} \right\} = \tau_{\max} \cdot \left(1 - \frac{(r - r')\cos\varphi}{R'} \right) \left(\frac{r}{r_0} \right)^{\lambda_3 - 1} \left\{ \begin{array}{l} \sin\lambda_3\varphi \\ \cos\lambda_3\varphi \end{array} \right\}, \tag{109}$$

where

$$r' = \left(\frac{u_0}{\cos(\varphi/q)} \right)^q = \frac{r_0}{(\cos(\varphi/q))^q} \tag{110}$$

is the value of the polar coordinate r when evaluated on the notch edge

$$R' = R + (r_0 - r'\cos\varphi) \tag{111}$$

and R is the radius of the net section of the shaft. Eqs. (110) and (111) are valid for $\varphi \neq \pm\gamma$.

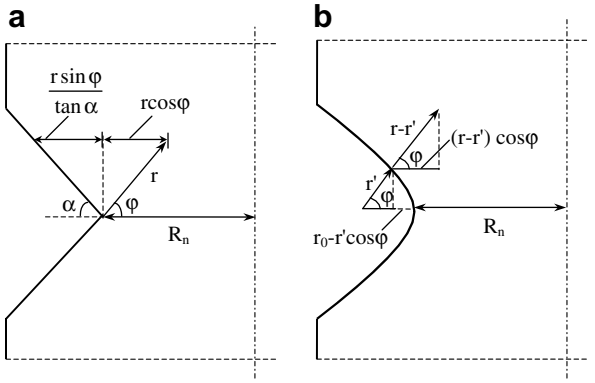

Fig. 10. Geometrical relationships to determine the correction factor taking into account the linear decrease of the nominal shear stress; (a) sharp V-notch; (b) rounded hyperbolic–parabolic notch.

In order to correctly account for the linear decrease of the nominal stress the definition of the generalised stress intensity factor should be updated in the following way:

$$K_{3\rho} = \frac{\sqrt{2\pi}}{1-\frac{r-r_0}{R}} \lim_{r\to r_o^+} [r^{1-\lambda_3}\tau_{z\varphi}(r,\varphi=0)]. \tag{112}$$

4.7. An estimation of the maximum shear stress for deep parabolic or hyperbolic notches under torsion loading

The maximum shear stress can be determined by imposing the equilibrium condition on the net section. Along the notch bisector line, it is possible to write:

$$\tau_{z\varphi}|_{y=0} = \tau_{zy}|_{y=0} = \tau_{\max}\left(\frac{x}{r_0}\right)^{\lambda_3-1}\left(1-\frac{x-r_0}{R}\right). \tag{113}$$

Introducing the auxiliary variable t, being

$$t = R + r_0 - x, \tag{114}$$

we can re-write Eq. (113) in the form:

$$\tau_{zy}|_{y=0} = \tau_{\max}\left(\frac{R+r_0-t}{r_0}\right)^{\lambda_3-1}\frac{t}{R}. \tag{115}$$

Considering a polar coordinate system (t,θ,z) centred on the axis of the shaft, we can write the equilibrium equation on the net section by equating the contribution given by the τ_{zy} stress and that due to the nominal shear stress τ_{nom}, ranging from τ^* to 0:

$$\int_A \tau(t)t\,\mathrm{d}A = \int_A \tau_{zy}|_{y=0}t\,\mathrm{d}A, \tag{116}$$

$$\int_0^{2\pi}\int_0^R \tau^*\frac{t^3}{R}\,\mathrm{d}t\,\mathrm{d}\theta = \int_0^{2\pi}\int_0^R \tau_{\max}\left(\frac{R+r_0-t}{r_0}\right)^{\lambda_3-1}\frac{t^3}{R}\,\mathrm{d}t\,\mathrm{d}\theta \tag{117}$$

and so

$$K_{\text{t,net}} = \frac{\frac{R^4}{4}}{\int_0^R\left(\frac{R+r_0-t}{r_0}\right)^{\lambda_3-1}t^3\,\mathrm{d}t}, \tag{118}$$

By means of some algebraic manipulations the stress concentration factor turns out to be:

$$K_{\text{t,net}} = \frac{s_3^4+10s_3^3+35s_3^2+50s_3+24}{4\sum_{j=0}^{3} I_j}, \tag{119}$$

where

$$\begin{aligned} &s_3(2\alpha) = \lambda_3 - 1,\\ &k(r_0,R) = \frac{r_0}{R},\\ &I_0 = \left(1+\frac{1}{k}\right)^{s_3}\left[6+24k+36k^2+24k^3+6k^4\right],\\ &I_1 = -k(24+26s_3+9s_3^2+s_3^3),\\ &I_2 = -k^2(36+21s_3+3s_3^2),\\ &I_3 = -k^3(24+6s_3)-6k^4. \end{aligned} \tag{120}$$

Note that, as expected, the stress concentration factor depends on the relevant geometric parameters characterising the notched shaft, that is the notch-opening angle, 2α, and $\frac{\rho}{R}$, the ratio of the notch root radius to the net shaft radius.

Recently, Noda and Takase (2006) analysed the stress concentration factors K_t of a round bar with rounded V-notches under torsion by means of the body force method. They initially considered the limiting cases of deep (K_{td}) and shallow (K_{ts}) notches and then classified the notches into four groups depending on notch radius and notch depth (blunt, sharp, shallow and deep notches). Afterwards, focusing attention on the case $2\alpha = 60°$, they proved that when the ratio between the notch depth to the gross section radius is equal to or greater than 0.2 and, at the same time, the net radius to the notch root radius ratio ranges between 0 and 20, K_t can be determined within 2 percent error, by using K_{td} (Noda and Takase, 2006, Fig. 7, pp. 156–157). These authors also address the effect of the notch-opening angle 2α on the theoretical stress concentration factor

Table 1
Comparison between K_t values as obtained by Neuber (1958) and Noda and Takase (2006) and by means of Eq. (119) of the present paper

ρ/R	R/ρ	$K_{t\ Neuber}$ Eq. (60)	$K_{t\ Noda-Takase}$				K_t – Eq. (119)				Δ (%)		
			2α	0°	60°	90°	0°	60°	90°	135°	0°	60°	90°
0.10	10.00	1.831		1.979	1.908	1.864	1.892	1.781	1.696	1.495	−4.4	−6.6	−9.0
0.20	5.00	1.513		1.573	1.560	1.539	1.559	1.505	1.461	1.349	−0.9	−3.5	−5.0
0.30	3.33	1.379		1.417	1.413	1.403	1.418	1.384	1.355	1.278	0.1	−2.1	−3.4
0.40	2.50	1.304		1.327	1.327	1.322	1.337	1.313	1.292	1.235	0.8	−1.1	−2.2
0.50	2.00	1.254		1.272	1.272	1.268	1.284	1.265	1.250	1.204	1.0	−0.5	−1.4
0.60	1.67	1.219		1.232	1.232	1.231	1.246	1.231	1.219	1.182	1.1	−0.1	−1.0
0.70	1.43	1.192		1.203	1.203	1.202	1.217	1.205	1.195	1.164	1.2	0.2	−0.6
0.80	1.25	1.172		1.181	1.181	1.180	1.195	1.185	1.176	1.150	1.2	0.3	−0.3
0.90	1.11	1.155		1.163	1.163	1.162	1.177	1.168	1.161	1.138	1.2	0.4	−0.1
1.00	1.00	1.142		1.148	1.148	1.148	1.162	1.155	1.148	1.128	1.3	0.6	0.1
1.11	0.90	1.129		1.135	1.134	1.135	1.148	1.142	1.136	1.119	1.2	0.7	0.1
1.25	0.80	1.117		1.121	1.121	1.121	1.134	1.129	1.124	1.109	1.1	0.7	0.3
1.43	0.70	1.103		1.108	1.108	1.108	1.119	1.115	1.111	1.099	1.0	0.6	0.3
1.67	0.60	1.090		1.093	1.093	1.093	1.104	1.101	1.098	1.088	1.0	0.7	0.4
2.00	0.50	1.076		1.078	1.078	1.078	1.088	1.086	1.084	1.076	0.9	0.7	0.5
2.50	0.40	1.062		1.063	1.063	1.063	1.072	1.071	1.069	1.063	0.9	0.7	0.6
3.33	0.30	1.047		1.048	1.048	1.048	1.055	1.054	1.053	1.050	0.7	0.6	0.5
5.00	0.20	1.032		1.032	1.032	1.032	1.038	1.037	1.037	1.035	0.6	0.5	0.5
10.00	0.10	1.016		1.017	1.017	1.017	1.019	1.019	1.019	1.019	0.2	0.2	0.2

Deep notches with notch-opening angle 2α. Differences Δ determined according to the expression $\Delta\% = (K_t, \text{Eq. } 119/K_{t,\ Noda-Takase} - 1) \times 100$.

for deep and shallow notches, with 2α ranging from 0 to 90°. This effect was found to be '*not very large*' for deep notches (the maximum difference between $2\alpha = 0$ and $2\alpha = 90°$ being 7%) but important for shallow notches; in both cases the differences increase as ρ decreases. Finally, they provided a set of formulae for K_t of any shape of notch with $2\alpha = 60°$ in a round bar under torsion, the errors being less than 1% with respect to the numerical results.

A comparison between the K_t values obtained by Neuber's formula, Eq. (60), by Eq. (119) and as reported by Noda and Takase (2006), Table 5, where the ratio between their K_t and Nueber's K_t for hyperbolic notches is listed is shown in Table 1 for $2\alpha = 0$, 60°, 90°; in addition the K_t values for $2\alpha = 135°$ are also listed, as obtained by Eq. (119). The comparison is limited here to deep notches, i.e., to notches where the ratio between the notch depth and the gross section radius tends to unity, according to Noda and Takase (2006). The agreement is very satisfactory when ρ/R is equal to or greater than 0.5, the maximum difference being about 1.5%. As ρ/R decreases the difference increases, mainly due to the different notch shape, V-notches and hyperbolic notches. Furthermore, it can be noted that the influence of the notch-opening angle is evident for small values of ρ/R, in agreement with Noda and Takase (2006), while it is very low for high values of ρ/R.

4.8. An estimation of the maximum shear stress for deep parabolic or hyperbolic notches in the case of uniform antiplane shear

In the same way, it is possible to determine the stress concentration factor for uniform antiplane shear. In this case stresses do not decrease linearly across the section and so the equilibrium equation becomes:

$$\int_0^{2\pi}\int_0^R \tau^* t^2\,\mathrm{d}t\,\mathrm{d}\theta = \int_0^{2\pi}\int_0^R \tau_{max}\left(\frac{R+r_0-t}{r_0}\right)^{\lambda_3-1} t^2\,\mathrm{d}t\,\mathrm{d}\theta \tag{121}$$

$$K_{t,net} = \frac{\frac{R^3}{3}}{\int_0^R \left(\frac{R+r_0-t}{r_0}\right)^{\lambda_3-1} t^2\,\mathrm{d}t}, \tag{122}$$

that is

$$K_{t,net} = \frac{s_3^3 + 6s_3^2 + 11s + 6}{3(I_0 + I_1)}, \tag{123}$$

where

$$\begin{aligned} s_3(2\alpha) &= \lambda_3 - 1,\\ k(\rho,R) &= \frac{r_0}{R},\\ I_0 &= 2\left(1+\frac{1}{k}\right)^{s_3}(1+k)^3,\\ I_1 &= -k(s_3+3)(s_3+2) - 2k^2(s_3+3) - 2k^3 \end{aligned} \tag{124}$$

4.9. The influence of finite dimensions on stress distributions

In an infinite body, stress distributions are not influenced by external boundary and depend only on the relevant boundaries conditions provided by the notch shape. As the absolute dimensions decrease the outer boundaries have a greater influence.

Despite this fact, recalling Williams (1952, 1957), stresses ahead of a notch in a component of finite dimension can be written as the sum of two terms, the leading order one, due to the notch shape, and the resultant of all the higher order ones, which depends also on the global geometry. This problem was recently discussed also by Dini and Hills (2004) dealing with notches under Mode I loading. Furthermore, it can be observed that, in the infinite solution, only the leading term remains.

So the stress distribution for a finite-depth hyperbolic or parabolic notch in a round shaft under torsion can be determined as:

$$\left\{ \begin{array}{c} \tau_{zr}(r,\varphi) \\ \tau_{z\varphi}(r,\varphi) \end{array} \right\} = \tau_{\max} \cdot \left(1 - \frac{(r-r')\cos\varphi}{R'}\right)\left(\frac{r}{r_0}\right)^{\lambda_3 - 1} \left\{ \begin{array}{c} \sin\lambda_3\varphi \\ \cos\lambda_3\varphi \end{array} \right\} + \text{higher order terms.} \tag{125}$$

Stresses ahead of the notch can be successfully determined simply ignoring the contribution due to the higher order terms that become less meaningful as r tends to r_0:

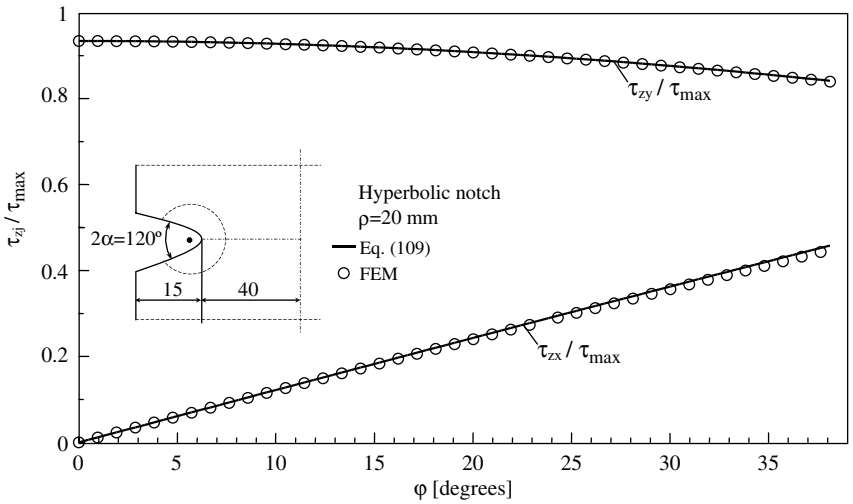

Fig. 11. Stress fields plotted along a circular path of radius $r = 6.3$ mm centred on the notch focus; stresses normalised with respect to the maximum shear stress (hyperbolic notch).

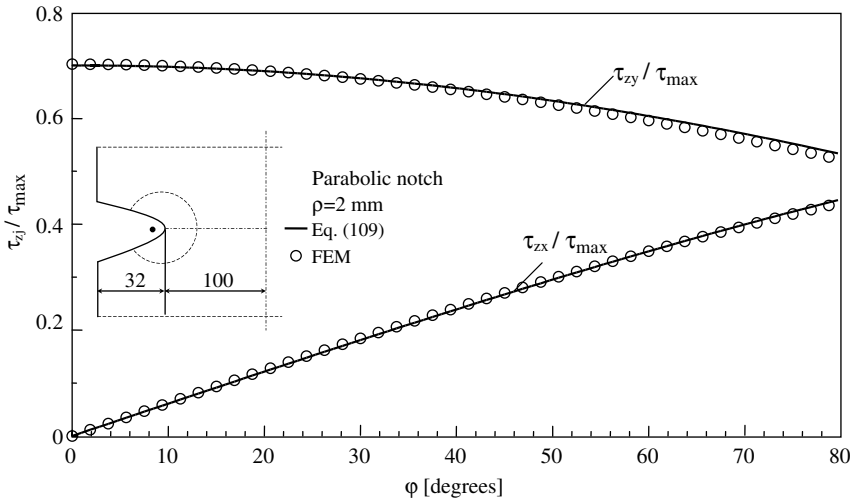

Fig. 12. Stress fields plotted along a circular path of radius $r = 2$ mm centred on the notch focus; stresses normalised with respect to the maximum shear stress (parabolic notch).

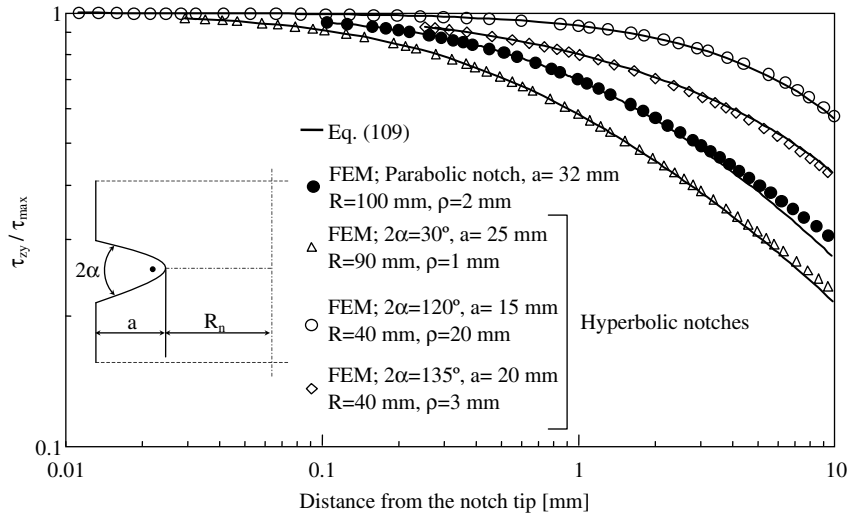

Fig. 13. Plot of the stress component τ_{zy} along the notch bisector line. The stress component is normalised with respect to the maximum shear stress (hyperbolic and parabolic notches).

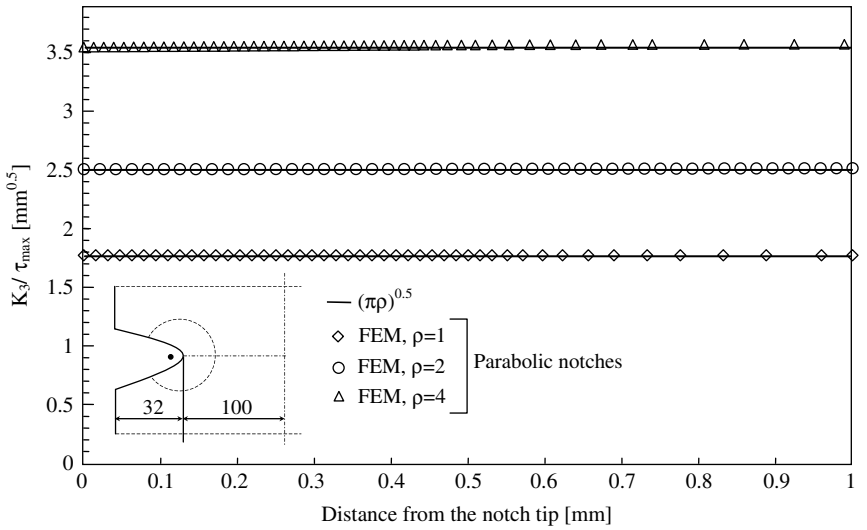

Fig. 14. Comparison between Eq. (103) and FEA results (parabolic notch).

$$\begin{Bmatrix} \tau_{zr}(r,\varphi) \\ \tau_{z\varphi}(r,\varphi) \end{Bmatrix} \cong \tau_{\max} \cdot \left(1 - \frac{(r-r')\cos\varphi}{R'}\right)\left(\frac{r}{r_0}\right)^{\lambda_3 - 1} \begin{Bmatrix} \sin\lambda_3\varphi \\ \cos\lambda_3\varphi \end{Bmatrix}. \tag{126}$$

With this simplification Eq. (126), when applied to a finite notch, is valid only in the vicinity of the notch tip; that is in the highly stressed regions. This result agrees with those of other researchers (Williams, 1952, 1957; Lazzarin and Tovo, 1996).

4.10. A comparison with numerical results

In principle Eq. (109) is valid only for infinite gross section shafts. Nevertheless, as stated above, it remains efficient even in the highly stressed regions of finite shafts. Figs. 11–13 show the results of a number of finite element analyses carried out on finite shafts weakened by hyperbolic and parabolic notches; there is a good agreement between numerical results and Eq. (109). Fig. 14 shows a comparison between Eq. (103) and FEA results.

5. Limitations and applicability ranges of the two classes of solutions proposed

It is now interesting to do a comparison between the two solutions obtained using two different transformations and to discuss the applicability of each of them.

The first solution, obtained using the hyperbolic transformation, has been demonstrated to be valid over the entire ligament. Unfortunately, it is applicable only to very deep hyperbolic notches or to notches with a large root radius. Moreover, choosing the notch-opening angle $2\alpha = 2\eta_0$ and the notch root radius results in automatically fixing the net radius of the section:

$$a = \frac{\rho}{\tan^2 \eta_0}, \tag{127}$$

limiting the degrees of freedom for applications. Even if mathematically obtained for infinite shafts, it can also be applied to finite shafts, especially to estimate stress components along the notch bisector line.

In contrast, the second solution, which is exact for infinite bodies, needs no assumptions for the notch root radius, the opening angle or the size of the net section, being a general solution able to describe a large range of notch shapes. Furthermore, when applied to finite-depth notches, it remains effective in the highly stressed region close to the notch tip.

6. An explicit link between plane and antiplane elasticity problems

According to Muskhelishvili's method (Muskhelishvili, 1977), stress components in the proximity of a notch or a crack under plane stress–strain can be determined using the following expressions:

$$\begin{aligned} &\sigma_{xx} + \sigma_{yy} = 4Re\psi'(z), \\ &\sigma_{xx} - \sigma_{yy} - 2i\tau_{zy} = 2[z\bar{\psi}''(\bar{z}) + \bar{\chi}''(\bar{z})], \end{aligned} \tag{128}$$

where, as well known, ψ and χ are two holomorphic functions.

For the same notch profile, the hyperbolic notch for example, the plane problem and the antiplane one cannot be uncoupled, the stresses being essentially a geometric problem. As a consequence there must be a precise link between the holomorphic functions used in the two cases.

Indeed, it can be demonstrated that the two functions $H(z)$ and ψ (z) have the same form. This agrees with the results recently obtained by Lazzarin et al. (2007), for a semi-elliptic notch, and those obtained in this work.

7. Averaged strain energy density

The concept of 'elementary volume', introduced many years ago by Neuber (1958), has been reconsidered in some recent papers where the strain energy density (SED) was evaluated over a given finite size volume surrounding the tip of sharp and blunt V-notches subjected to Mode I loading. By using the mean value of the SED, the static strength properties of brittle components weakened by sharp and blunt V-notches subject to Mode I (Lazzarin and Berto, 2005) or and mixed mode, I + II, loading (Gómez et al., 2007) were determined in a unified manner, as were the high cycle fatigue strength properties of welded joints made of steels or aluminium alloys (Livieri and Lazzarin, 2005; Lazzarin et al., 2008). The control volume suggested in (Lazzarin and Berto, 2005) adapts itself as a function of the notch root radius ρ and the opening angle 2α, whereas its maximum width, measured along the notch bisector line, equals R_C, a material parameter which works like Neuber's 'microstructural support length (see Fig. 15). In parallel, dealing with U- and V-shaped notches under Mode I loading, a bridging between the elastic strain energy and the J-integral has been underlined by using the same control volume (Berto and Lazzarin, 2007).

The aim of this section is to provide some closed-form expressions for the mean value of the strain energy density in the presence of blunt notches under Mode III loading. These analytical results are intended to be the basis for further investigations on the static strength properties of both sharp and blunt notched components under Mode III, as well as the possible links between the SED and the J-integral for blunt notches under Mode III.

By taking advantage of Eq. (96) the total energy evaluated over a circular sector embracing the notch tip (see Fig. 15) can be determined as:

$$\begin{aligned} E_3 &= \frac{(1+\nu)}{E}\tau_{max}^2\left(\frac{1}{r_0}\right)^{2(\lambda_3-1)}\int_{-\bar{\varphi}}^{+\bar{\varphi}}\int_{R_1(\varphi)}^{R_2(\varphi)} r^{2(\lambda_3-1)} r\,dr\,d\varphi = \frac{(1+\nu)}{E}\cdot\frac{\tau_{max}^2}{r_0^{2(\lambda_3-1)}}\int_{-\bar{\varphi}}^{+\bar{\varphi}}\frac{R_2^{2\lambda_3}(\varphi)-R_1^{2\lambda_3}(\varphi)}{2\lambda_3}d\varphi \\ &= \frac{(1+\nu)}{E\lambda_3}\cdot\frac{\tau_{max}^2\cdot I_3}{r_0^{2(\lambda_3-1)}}, \end{aligned} \tag{129}$$

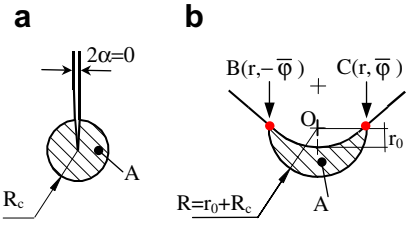

Fig. 15. Control volume (area) in the evaluation of the averaged strain energy density for a crack (a) and a blunt notch (b).

where

$$I_3 = \int_{-\bar{\varphi}}^{+\bar{\varphi}} \frac{R_2^{2\lambda_3}(\varphi) - R_1^{2\lambda_3}(\varphi)}{2} \mathrm{d}\varphi. \tag{130}$$

The averaging volume Ω can be determined by means of the following expression:

$$\Omega = \int_{-\bar{\varphi}}^{+\bar{\varphi}} \int_{R_1(\varphi)}^{R_2(\varphi)} r \mathrm{d}r \mathrm{d}\varphi = \int_{-\bar{\varphi}}^{+\bar{\varphi}} \frac{R_2^2(\varphi) - R_1^2(\varphi)}{2} \mathrm{d}\varphi. \tag{131}$$

It is evident (see Fig. 15) that Ω is included between two radius: an outer radius R_2 which is constant and equal to:

$$R_2 = r_0 + R_C = \rho\left(\frac{q-1}{q} + \frac{R_C}{\rho}\right) \tag{132}$$

and an inner radius R_1 which is a function of the polar angle φ according to the following expression:

$$R_1(\varphi) = \frac{r_0}{\left(\cos\left(\frac{\varphi}{q}\right)\right)^q} = \rho \frac{\frac{q-1}{q}}{\left(\cos\left(\frac{\varphi}{q}\right)\right)^q}. \tag{133}$$

Then, the averaged strain energy density over the volume Ω turns out to be:

$$\overline{W}_3 = \frac{E_3}{\Omega} = \frac{(1+\nu)}{E\lambda_3} \cdot \frac{\tau_{\max}^2}{r_0^{2(\lambda_3-1)}} \frac{I_3}{\Omega} = \frac{\tau_{\max}^2}{2G} h_3\left(2\alpha, \frac{R_C}{\rho}\right), \tag{134}$$

where

$$h_3\left(2\alpha, \frac{R_C}{\rho}\right) = \frac{1}{\lambda_3(1-\lambda_3)^{2(\lambda_3-1)}} \frac{2\int_0^{\bar{\varphi}} \left\{\left[\frac{q-1}{q} + \frac{R_C}{\rho}\right]^{2\lambda_3} - \left[\frac{q-1}{q} \cdot \left(\cos\left(\frac{\varphi}{q}\right)\right)^{-q}\right]^{2\lambda_3}\right\} d\varphi}{2\int_0^{\bar{\varphi}} \left\{\left[\frac{q-1}{q} + \frac{R_C}{\rho}\right]^{2} - \left[\frac{q-1}{q} \cdot \left(\cos\left(\frac{\varphi}{q}\right)\right)^{-q}\right]^{2}\right\} \mathrm{d}\varphi}. \tag{135}$$

The limit angle $\bar{\varphi}$ can be written as a function of the material-dependent radius R_C to the root radius ρ ratio, by means of the following relationship:

$$\bar{\varphi} = \frac{1}{\lambda_3} \cdot \arccos\left[\left(\frac{1-\lambda_3}{1-\lambda_3+\frac{R_C}{\rho}}\right)^{\lambda_3}\right]. \tag{136}$$

In general, analytical solution of Eq. (135) involves Euler Gamma functions and hypergeometric functions; then for the sake of simplicity h_3 is listed in Table 2 for some value of 2α and R_C/ρ.

However, for the simple case of a parabolic notch Eqs. (135) and (136) simplify as follows:

$$h_3\left(2\alpha, \frac{R_C}{\rho}\right) = \frac{\left(\frac{1}{2} + \frac{R_C}{\rho}\right)\bar{\varphi} - \tan\frac{\bar{\varphi}}{2}}{\left(\frac{1}{2} + \frac{R_C}{\rho}\right)^2 \bar{\varphi} - \frac{1}{6}\tan\frac{\bar{\varphi}}{2}\left(2 + \sec^2\frac{\bar{\varphi}}{2}\right)}, \tag{137}$$

$$\bar{\varphi} = 2 \cdot \arccos\left[\sqrt{\frac{1}{1+2\frac{R_C}{\rho}}}\right]. \tag{138}$$

Table 2
Values of the function h_3 for some opening angles 2α and some R_C/ρ ratios

$2\alpha R_C/\rho$	h_3					
	0°	45°	60°	90°	120°	135°
0.01	0.98815	0.98816	0.98817	0.98818	0.98822	0.98825
0.05	0.94359	0.94384	0.94396	0.94433	0.94505	0.94574
0.10	0.89352	0.89439	0.89482	0.89606	0.89846	0.90072
0.20	0.80847	0.81114	0.81244	0.81620	0.82319	0.82954
0.30	0.73883	0.74358	0.74587	0.75246	0.76443	0.77504
0.40	0.68067	0.68751	0.69079	0.70014	0.71688	0.73148
0.50	0.63132	0.64012	0.64433	0.65625	0.67735	0.69547
0.75	0.53525	0.54822	0.55438	0.57169	0.60178	0.62712
1.00	0.46524	0.48136	0.48899	0.51033	0.54714	0.57782
2.50	0.26324	0.28681	0.29802	0.32947	0.38385	0.42909
5.00	0.15430	0.17828	0.18992	0.22330	0.28298	0.33405
10.00	0.08512	0.10570	0.11604	0.14676	0.20483	0.25692

It is evident that the averaged strain energy density is a fraction of the maximum strain energy density at the notch tip. For values of R_C/ρ less than 0.1 (that is when the notch root radius is large in comparison with the radius R_C or, on the contrary, when the averaging volume is very small and close to the notch tip) the averaged strain energy density is less than 10% smaller than the peak energy.

8. Conclusions

Closed-form solutions for the stress fields induced by circumferential notches of different shape in axisymmetric shafts under torsion and uniform antiplane shear have been developed. The boundary value problems have been formulated by means of complex potential functions in combination with two different coordinate systems, providing two classes of solutions.

The former solution, obtained using the hyperbolic transformation, is applicable only to very deep hyperbolic notches or to notches with a large root radius, and this fact limits its use in engineering applications.

The latter solution, obtained by using Neuber's transformation, is more flexible since it requires no restrictions on the notch root radius, the opening angle or the net section diameter. This solution is suitable for describing a wide range of notch shapes and has the merit to match some well-known solutions of linear elastic fracture and notch mechanics.

It has also been demonstrated that the contribution of higher order terms of stress distributions, due the finite size effect, does not change the stress distribution shape in the highly stressed region ahead of the notch tip. Due to this fact, the analytical results obtained for the shear stresses show a good agreement with numerical results both for infinite and finite size round bars. Finally, the developed analytical frame has allowed us to link the generalised N-SIFs to the maximum shear stress at the notch tip and to give closed-form expressions for the strain energy density over a given control volume embracing the notch tip.

Appendix A. An analytical link between the distributions of different kind of notches under torsion

Consider the expression of τ_{zy} along the notch bisector line of a semi-elliptic notch (Lazzarin et al., 2007), neglecting the linear decrease of the nominal shear stress:

$$\tau_{zy} = \frac{b\tau_{\max}}{a^2 - b^2}\left(\frac{ax}{\sqrt{x^2 - c^2}} - b\right). \tag{A1}$$

If x' is the distance from the notch tip, then $x' = x - a$ and:

$$\tau_{zy} = \frac{b\tau_{\max}}{a^2 - b^2}\left(\frac{a(x' + a)}{\sqrt{(x' + a)^2 - c^2}} - b\right). \tag{A2}$$

After some algebraic manipulations Eq. (A2) can be written in a different way, Eq. (A3), bearing in mind that $\rho = \frac{b^2}{a}$, $\frac{a^2}{b^2} = \frac{a}{\rho}$, $c^2 = a^2 - b^2$:

$$\begin{aligned}\tau_{zy} &= \frac{ba\tau_{\max}}{a^2(1 - \frac{b^2}{a^2})}\left(\frac{(x' + a)}{\sqrt{(x' + a)^2 - c^2}} - \frac{b}{a}\right) = \sqrt{\frac{\rho}{a}} \cdot \frac{\tau_{\max}}{(1 - \frac{\rho}{a})}\left(\frac{(x' + a)}{\sqrt{x'^2 + 2ax' + b^2}} - \sqrt{\frac{\rho}{a}}\right) \\ &= \frac{\tau_{\max}}{(1 - \frac{\rho}{a})}\left(\frac{\frac{x'}{a} + 1}{\sqrt{\frac{x'^2}{a\rho} + 2\frac{x'}{\rho} + 1}} - \frac{\rho}{a}\right).\end{aligned} \tag{A3}$$

Now, if $a \gg \rho$ and $x' \ll a$, Eq. (A3) tends to the following expression:

$$\tau_{zy} = \tau_{\max}\left(\frac{1}{\sqrt{2\frac{x'}{\rho} + 1}}\right), \tag{A4}$$

and so exactly matches Eq. (102), valid for a slim parabolic notch.

Consider now Eq. (55) valid for a deep hyperbolic notch. Neglecting again the linear decrease of the nominal shear stress:

$$\tau_{zy}|_{\xi=0} = \frac{b\tau_{\max}}{\sqrt{c^2 - x^2}}. \tag{A5}$$

If x' is the distance from the notch tip, then $x' = a - x$ and so, remembering also that $c^2 = a^2 + b^2$, one obtains:

$$\tau_{zy} = \frac{b\tau_{\max}}{\sqrt{a^2 + b^2 - x'^2 - a^2 + 2ax'}} = \frac{\tau_{\max}}{\sqrt{1 - \frac{x'^2}{b^2} + \frac{2ax'}{b^2}}}. \tag{A6}$$

Finally, if $a \gg \rho$ and $x' \ll a$, being $\rho = \frac{b^2}{a}$, the expression becomes:

$$\tau_{zy} = \tau_{\max}\left(\frac{1}{\sqrt{2\frac{x'}{\rho}+1}}\right), \tag{A7}$$

according to the expression valid for a parabolic notch.

References

Atzori, B., Lazzarin, P., Tovo, R., 1997. Stress distributions for V-shaped notches under tensile and bending loading. Fatigue Fract. Eng. Mater. Struct. 20, 1083–1092.

Atzori, B., Lazzarin, P., Filippi, S., 2001. Cracks and notches, analogies and differences of the relevant stress distributions and practical consequences in fatigue limit predictions. Int. J. Fatigue 23, 355–362.

Berto, F., Lazzarin, P., 2007. Relationships between *J*-integral and the strain energy evaluated in a finite volume surrounding the tip of sharp and blunt V-notches. Int. J. Solids Struct. 44, 4621–4645.

Creager, M., Paris, P.C., 1967. Elastic field equations for blunt cracks with reference to stress corrosion cracking. Int. J. Fract. Mech. 3, 247–252.

Dini, D., Hills, D.A., 2004. Asymptotic characterisation of nearly-sharp notch root stress fields. Int. J. Fract. 130, 651–666.

Dini, D., Hills, D.A., 2006. When does a notch behaves like a crack? In: Proceedings of the I MECH E Part CJ. Mech. Eng. Sci., vol. 220, pp. 27–43.

Dunn, M.L., Suwito, W., Cunningham, S., 1997. Stress intensities at notch singularities. Eng. Fract. Mech. 57, 417–430.

England, A.H., 1971. On stress singularities in linear elasticity. Int. J. Eng. Sci. 9, 571–585.

Filippi, S., Lazzarin, P., Tovo, R., 2002. Developments of some explicit formulas useful to describe elastic stress fields ahead of notches in plates. Int. J. Solids Struct. 39, 4543–4565.

Filon, L.N.G., 1900. On the resistance to torsion of certain forms of shafting with special reference to the effect of keyways. Phil. Trans. R. Soc. Lond. A 193, 309–352.

Glinka, G., 1985. Calculation of inelastic notch-tip strain–stress histories under cyclic loading. Eng. Fract. Mech. 22, 839–854.

Gómez, F.J., Elices, M., Berto, F., Lazzarin, P., 2007. Local strain energy to assess the static failure of U-notches in plates under mixed mode loading. Int. J. Fract. 145, 29–45.

Gross, R., Mendelson, A., 1972. Plane elastostatic analysis of V-notched plates. Int. J. Fract. Mech. 8, 267–276.

Hamada, M., Kitagawa, H., 1968. Numerical solutions of two-dimensional elastic plastic problems by conformal mapping and finite difference method (elastic torsion of circumferentially grooved shafts). Bull. Jpn. Soc. Mech. Eng. 11, 605–611.

Hasebe, N., Kutanda, Y., 1978. Calculation of stress intensity factor from stress concentration factor. Eng. Fract. Mech. 10, 215–221.

Inglis, C.E., 1913. Stresses in a plate due to the presence of cracks and sharp corners. Trans. Inst. Naval Architects 55, 219–230.

Lazzarin, P., Berto, F., 2005. Some expressions for the strain energy in a finite volume surrounding the root of blunt V-notches. Int. J. Fract. 135, 161–185.

Lazzarin, P., Filippi, S., 2006. A generalised stress intensity factor to be applied to rounded V-shaped notches. Int. J. Solids Struct. 43, 2461–2478.

Lazzarin, L., Tovo, R., 1996. A unified approach to the evaluation of linear elastic stress fields in the neighborhood of cracks and notches. Int. J. Fract. 78, 3–19.

Lazzarin, P., Zappalorto, M., Yates, J.R., 2007. Analytical study of stress distributions due to semi-elliptic notches in shafts under torsion loading. Int. J. Eng. Sci. 45 (2–8), 308–328.

Lazzarin, P., Livieri, P., Berto, F., Zappalorto, M., 2008. Local strain energy density and fatigue strength of welded joints under uniaxial and multiaxial loading. Eng. Fract. Mech. 75, 1875–1889.

Livieri, P., Lazzarin, P., 2005. Fatigue strength of steel and aluminium welded joints based on generalised stress intensity factors and local strain energy values. Int. J. Fract. 133, 247–276.

Matthews, G.J., Hoke, C.J., 1971. Solution of axis-symmetric torsion problems by point matching. J. Strain. Anal. 6, 124–133.

Muskhelishvili, N.I., 1977. Some Basic Problems of the Mathematical Theory of Elasticity, fourth ed. Noordhoof International, Leyden, The Netherlands.

Neuber, H., 1958. Theory of Notch Stresses. Springer-Verlag, Berlin.

Noda, N., Takase, Y., 2003. Generalized stress intensity factors for V-shaped notch in a round bar under torsion, tension and bending. Eng. Fract. Mech. 70, 1447–1466.

Noda, N., Takase, Y., 2006. Stress concentration formula useful for all notch shape in a round bar (comparison between torsion, tension and bending). Int. J. Fatigue 28, 151–163.

Nui, L.S., Chehimi, C., Pluvinage, G., 1994. Stress field near a large blunted tip V-Notch and application of the concept of the critical notch stress intensity factor (NSIF) to the fracture toughness of very brittle materials. Eng. Fract. Mech. 49, 325–335.

Peterson, R.E., 1974. Stress Concentration Factors. John Wiley & Sons, New York.

Qian, J., Hasebe, N., 1997. Property of Eigenvalues and eigenfunctions for an interface V-notch in antiplane elasticity. Eng. Fract. Mech. 56, 729–734.

Rice, J.R., 1968. A path independent integral and the approximate analysis of strain concentration by notches and cracks. J. Appl. Mech. 35, 379–386.

Rushton, K.R., 1967. Stress concentrations arising in the torsion of grooved shafts. Int. J. Mech. Sci. 9, 697–705.

Seweryn, A., Molski, K., 1996. Elastic stress singularities and corresponding generalized stress intensity factors for angular corners under various boundary condition. Eng. Fract. Mech. 55, 529–556.

Shepherd, W.M., 1932. The torsion and flexure of shafting with keyways or cracks. Proc. R. Soc. Lond. 138, 607–634.

Smith, E., 2004a. The elastic stress distribution near the root of an elliptically cylindrical notch subjected to mode III loadings. Int. J. Eng. Sci. 42, 1831–1839.

Smith, E., 2004b. A comparison of Mode I and Mode III results for the elastic stress distribution in the immediate vicinity of a blunt notch. Int. J. Eng. Sci. 42, 473–481.

Smith, E., 2004c. A comparison of the Modes I and III elastic stress distribution near a circular cylindrical notch. Int. J. Eng. Sci. 42, 483–490.

Stevenson, A.C., 1945. Complex potentials in two-dimensional elasticity. Proc. R. Soc. Lond. A 184, 532–554.

Timoshenko, S.P., Goodier, J.N., 1970. Theory of Elasticity, third ed. McGraw-Hill, New York.

Wigglesworth, L.A., 1939. Flexure and torsion of an internally cracked shaft. Proc. R. Soc. Lond. 170, 365–391.

Wigglesworth, L.A., Stevenson, A.C., 1939. Flexure and torsion of cylinders with cross-sections bounded by orthogonal circular arcs. Proc. R. Soc. Lond. A184, 391–414.

Williams, M.L., 1952. Stress singularities resulting from various boundary conditions in angular corners of plate in extension. J. Appl. Mech. 19, 526–528.

Williams, M.L., 1957. On the stress distribution at the base of a stationary crack. J. Appl. Mech. 24, 109–114.